



Novel CuO–SiO₂ nanocomposites: synthesis, kinetics, recyclability, high stability and photocatalytic efficiency for Rose Bengal dye removal

Ahlam Hacine Gharbi^{1,2} · Hadia Hemmami^{1,2,3} · Salah Eddine Laouini^{1,4} · Abderrhmane Bouafia^{1,4} · Ilham Ben Amor^{1,2} · Soumeia Zeghoud^{1,2} · Mohammed Taher Gherbi^{3,5} · Asma Ben Amor^{1,2} · Fahad Alharthi⁶ · Johar Amin Ahmed Abdullah⁷

Received: 24 November 2023 / Accepted: 26 January 2024 / Published online: 26 February 2024
© The Author(s), under exclusive licence to Springer Nature Switzerland AG 2024

Abstract

A novel CuO–SiO₂ nanoadsorbent, incorporating copper oxide (CuO) and silicon dioxide (SiO₂), has been successfully synthesized using three distinct preparation processes: Mode-A (solution and solution), Mode-B (solution and nanoparticles), and Mode-C (nanoparticles and nanoparticles). The investigation focuses on evaluating the efficiency of the CuO–SiO₂ nanoadsorbent, considering its synthesis process, reusability, and sustained performance over time, particularly in the removal of Rose Bengal dye. Characterization results revealed the formation of CuO–SiO₂ nanocomposites structure irregular shapes morphology across all three-preparation processes. The average particle sizes for Mode-A, Mode-B, and Mode-C nanocomposites were determined as 18.1 nm, 15.6 nm, and 14.8 nm, respectively. Furthermore, the band gap energies of the CuO–SiO₂ nanocomposites were measured at 2.2 eV, 1.8 eV, and 3.29 eV for Mode-A, Mode-B, and Mode-C, respectively. Remarkably, the CuO–SiO₂ nanocomposite prepared using Mode-B demonstrated superior photocatalytic activity in degrading the anionic dye Rose Bengal, achieving a degradation coefficient of 84.8%. In comparison, CuO NPs, tested under the same experimental conditions (120 min contact time, pH = 7, temperature of 25 °C, and solar light irradiation), achieved a degradation coefficient of 78.8%. These findings highlight the potential of the CuO–SiO₂ nanoadsorbent, particularly when synthesized via Mode-B, for effective and environmentally friendly dye degradation applications.

✉ Abderrhmane Bouafia
abdelrahmanebouafia@gmail.com

Ahlam Hacine Gharbi
ahlam-hacinegharbi@univ-eloued.dz

Hadia Hemmami
hemmami-hadia@univ-eloued.dz

Salah Eddine Laouini
salah_laouini@yahoo.fr

Ilham Ben Amor
ilhambenamor97@gmail.com

Soumeia Zeghoud
zsoumeia@gmail.com

Mohammed Taher Gherbi
gherbi-mohammedtahir@univ-eloued.dz

Asma Ben Amor
benamor-asma@univ-eloued.dz

Fahad Alharthi
fharthi@ksu.edu.sa

Johar Amin Ahmed Abdullah
johabd@alum.us.es

¹ Department of Process Engineering and Petrochemical, Faculty of Technology, University of El Oued, P.O. Box 789, 39000 El Oued, Algeria

² Renewable Energy Development unit in Arid Zones (UDERZA), University of El Oued, P.O. Box 789, 39000 El Oued, Algeria

³ Laboratory of Applied Chemistry and Environment, Faculty of Exact Sciences, University of El Oued, P.O. Box 789, 39000 El Oued, Algeria

⁴ Laboratory of Biotechnology Biomaterial and condensed matter, Faculte de la Technologie, University of El Oued, P.O. Box 789, 39000 El Oued, Algeria

⁵ Department of Mechanical Engineering, University of El Oued, 39000 El Oued, Algeria

⁶ Department of Chemistry, College of Science, King Saud University, 11451 Riyadh, Kingdom of Saudi Arabia

⁷ Departamento de Ingeniería Química, Escuela Politécnica Superior, Universidad de Sevilla, 41012 Seville, Spain

Introduction

Nanotechnology and nanoscience, in the field of materials science, deal with particles sized from 1 to 100 nm, resulting in a high surface-to-volume ratio [1, 2]. Nanoparticles (NPs) have precise, controllable properties at atomic levels, benefiting electronics, optoelectronics, agriculture, communications, and biomedicine sectors [3, 4]. Copper oxide nanoparticles (CuO) stand out among other nanoparticles (NPs) due to their exceptional properties, including high chemical stability, excellent photostability, a high electrochemical coupling coefficient, and broad radiation absorption spectrum, garnering significant attention [5].

CuO NPs, with a wide direct band gap (1.2–2.1 eV) and classification as p-type semiconductors in group II–VI, demonstrate promise in multiple fields such as agriculture, pharmaceuticals, biology, and environmental science, owing to their unique characteristics and monoclinic crystal structures [6, 7]. Additionally, CuO NPs provide several advantages, including low toxicity, high chemical and thermal stability, compatibility, ease of synthesis, diverse nanoscale morphologies, a high specific surface area, enhanced oxygen adsorption capacity, and cost-effectiveness [8–10]. CuO NPs have significant photocatalytic potential but can be improved by modifying their structure with various elements, enhancing their photocatalytic activity and applications in photocatalysis [11]. Increasing stability of magnetic nanoparticles involves diverse methods like carbon, noble metals, metal oxides, and chitosan modifications. Silica (SiO₂) coating serves to reduce toxicity, enhance stability, promote biodegradability and biocompatibility, and prevent nanoparticle aggregation [12]. SiO₂ NPs have applications in electronics, drug delivery, and catalysis for hazardous pollutants [13]. For increased porosity, SiO₂ NPs are sometimes combined with other materials [14, 15]. Several silica-based nanocomposites have been developed, including Ag/SiO₂ [16], PdNi/C [17], Au@SiO₂, and SiO₂@Au core-shell [18], SiO₂@Au@GO [19], Zr-SiO₂ [20], NiO/SiO₂ [21], CuO-SiO₂ [22], Al₂O₃-SiO₂ [23], TiO₂-SiO₂-S [24], Al₂O₃-SiO₂-MgO [25], CoFe₂O₄/SiO₂ [26], and Fe₃O₄-SiO₂ [27], each offering unique properties and diverse applications.

CuO-SiO₂ nanocomposites are highly sought after due to their exceptional electrical, optical, and catalytic properties, garnering significant interest across scientific disciplines [28, 29]. Their synthesis requires precise control, involving careful technique selection and reactant mixing method optimization [22]. The integration of CuO NPs and SiO₂ NPs in water treatment technologies is pivotal for improving water quality and ensuring its safety for consumption. Additionally, addressing the challenge of dye removal from manufacturing and textile industry

effluents involves efficiently and environmentally friendly elimination or reduction of dye presence in wastewater [30]. Conventional dyeing processes frequently yield highly colored and potentially harmful effluents, underscoring the need for effective treatment methods to align with environmental standards and regulations. Among the numerous available techniques, three prominent methods stand out: adsorption, photocatalysis, and wave-induced treatment. Adsorption proves highly efficient in impurity removal using renewable materials, although it comes with associated maintenance costs [31]. Photocatalysis provides a rapid and residue-free solution, but its effectiveness may be light-dependent, and equipment costs can be substantial [32, 33]. Wave-induced treatment excels in swiftly breaking down pollutants, with considerations including energy costs and effectiveness on specific substances [34].

The textile industry is one of the largest consumers of water and chemicals, and it generates a significant amount of wastewater that contains dyes and other pollutants [35]. This wastewater can have a detrimental impact on aquatic life and human health [35]. Therefore, it is essential to treat the effluent before discharging it into the environment [36, 37].

There are several treatment methods available for removing dyes from industrial effluents, including biological, chemical, and physicochemical methods [35, 38]. Some of the commonly used techniques include adsorption, ion exchange, coagulation, filtration, photocatalytic oxidation, ozone, and Fenton's process [39, 40]. Advanced oxidation processes (AOP) such as ozonation, ultraviolet/hydrogen peroxide (UV/H₂O₂), anodic oxidation, and photocatalytic processes have also been employed to treat dye wastewater [39].

Despite the availability of several treatment methods, the challenge lies in selecting the most effective and cost-efficient method for a particular effluent. The efficacy of the treatment method depends on several factors, including the type of dye, the concentration of the dye, the pH of the effluent, and the presence of other pollutants [35]. Therefore, it is crucial to evaluate the effluent's characteristics and select the appropriate treatment method to achieve optimal results.

The novelty and importance of this work lie in its systematic exploration of various synthesis methods for CuO-SiO₂ nanocomposites and the thorough investigation of how different reactant mixing approaches influence material properties. Unlike previous works that may have focused on specific synthesis techniques, this study aims to provide a comprehensive understanding by examining multiple methods, each offering distinct advantages in controlling particle size, distribution, and crystallinity. By delving into mixing modes such as sequential addition and simultaneous mixing, the research seeks to uncover their specific impacts on nanocomposite homogeneity and chemical composition. The incorporation of advanced characterization techniques,

including X-ray diffraction (XRD), scanning electron microscopy (SEM), and spectroscopic analysis, adds depth to the structural, morphological, and elemental evaluation.

Furthermore, the study goes beyond the conventional scope by not only assessing the basic material properties but also delving into functional aspects such as catalytic activity and optical characteristics. This multifaceted approach is crucial in establishing correlations between synthesis parameters and the functional performance of CuO–SiO₂ nanocomposites. The inclusion of these additional analyzes enhances the understanding of the material's behavior in real-world applications, providing a more holistic view.

The anticipated contribution of this research is significant. By elucidating the intricate details of CuO–SiO₂ nanocomposite synthesis and reactant mixing optimization, the findings are expected to offer valuable insights. This knowledge, in turn, holds the promise of enabling the development of tailored nanocomposite materials with improved and finely tuned properties. The potential applications highlighted, such as the degradation of dyes through photocatalysis and environmental remediation, underscore the real-world impact of this work. Ultimately, the study aims to pave the way for more efficient and targeted solutions in various domains, addressing pressing challenges related to environmental sustainability and advanced materials science.

Materials and methods

Materials

Leaves of *Calligonumcomosum L.* and *Arachis hypogaea L.* were collected from El Oued, Algeria (33°22'06"N, 6°52'03"E). The experimental procedures involved the use of chemicals notable substances included Copper sulfate (CuSO₄·5H₂O, 98%), silica gel (hydrophilic-200 Silicon dioxide, 99.8%). Aladdin, 200 m²/g, < 100 mesh), Sodium hydroxide (NaOH, 97%), Hydrochloric acid (HCl, 98%), Sulfuric acid (H₂SO₄; 99%), Cupric acetate (Cu(Ac)₂, 98%), and Ammonium hydroxide. Rose Bengal (RB) dyes (C₂₀H₇Cl₄I₄Na₂O₅, > 99%) were purchased from Merck Germany. Additionally, distilled water and Whatman N°. 1 filter paper were employed in the process, and Biochem Chemophara as the manufacturer for all chemicals.

Preparation of plant extract

The fresh leaves of *Calligonum comosum L.* were initially rinsed with distilled water to eliminate impurities. Subsequently, they were air-dried in the shade at room temperature to eliminate any remaining moisture. Following this, a mixture consisting of 10 g of dried plant leaves and 150 ml of deionized water was boiled at 65 °C for 2 h. During the

boiling process, a light brown solution formed. The resulting browned extract was then filtered using Whatman No. 1 filter paper and stored in a refrigerator for future use [41].

Synthesis of CuO NPs

To synthesize CuO NPs using a leaf extract of *Calligonum comosum L.*, 50 ml of the plant leaf extract and 100 ml of 0.1 M CuSO₄·5H₂O were combined and continuously stirred at 70 °C for 2 h. While stirring, a 2 M NaOH solution was slowly added drop by drop to the mixture. The formation of copper oxide was confirmed by the observable color change from green to dark brown.

The precipitate was separated from the reaction solution through centrifugation at 3000 rpm for 10 min to eliminate impurities. Subsequently, the precipitate was dried at 80 °C for 24 h and then subjected to calcination at 600 °C for 6 h. The end product obtained was pale black CuO NPs [42].

Synthesis of SiO₂ NPs

The SiO₂ NPs synthesis was carried out in accordance with protocol [43]. Initially, ash was formed after peanut shells (*Arachis hypogaea L.*) were heated for two hours at a temperature between 600 and 700 °C. The mixture was then agitated at 70 °C for an hour while containing 10 g of ash and 100 ml of a 10% vol/vol HCl solution. Then the mixture was filtered, and the leftover material was removed using distilled water. After being dried for two hours at 70 °C, the resultant ash residue produced a white silica powder. The following step involved stirring 1 g of ash in 10 ml of a 2.5 N NaOH solution at 7–80 °C for 1h. After filtering the resultant solution, a 5 N·H₂SO₄ solution was used to titrate the filter. When the pH fell below 7, silica precipitated. After drying the precipitate, deionized water was added, and the result was amorphous SiO₂ NPs.

Synthesis of nanocomposite CuO–SiO₂ at different mixing modes of the reactants

Nanocomposite CuO–SiO₂ was prepared under similar conditions with different mixing modes of the reactants. Mode-A, Mode-B and Mode-C, The flow chart of the different mixing modes is given in Fig. 1.

Preparation of CuO–SiO₂ sample (Mode-A)

The CuO–SiO₂ sample was prepared by starting with a suspension of 1.0 g of dried silica gel (hydrophilic-200 Silicon dioxide (99.8%), Aladdin, 200 m²/g, < 100 mesh) in 50 mL of distilled water, along with a solution of cupric acetate (Cu(Ac)₂) (2 mL, 0.5 mol/L). The mixture was stirred at room temperature for 3 h. Subsequently, the Cu(Ac)₂

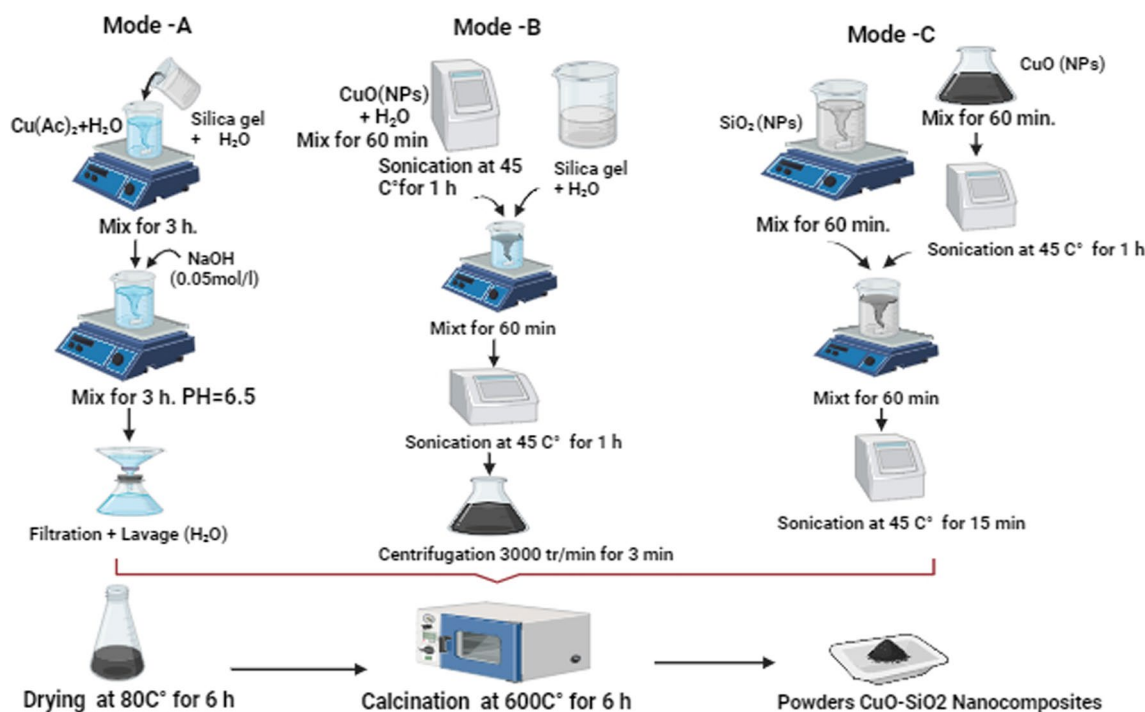


Fig. 1 The preparation of CuO–SiO₂ nanocomposites using various processes (Mode A, Mode B and Mode C)

solution was selectively precipitated by adding an aqueous solution of NaOH (0.05 mol/L) until the pH reached 6.5. The mixture was then stirred for an additional 3 h. After filtration, the resulting solid catalyst precursor was washed with distilled water until the pH reached 7, and then dried at 80 °C for 24 h. Finally, the CuO–SiO₂ sample was obtained by calcining the precursor in a furnace at 600 °C for 6 h [44].

Preparation of CuO–SiO₂ sample (Mode-B)

0.3 g of silica gel (hydrophilic-200 Silicon dioxide (99.8%), Aladdin, 200 m²/g, < 100 mesh) and 0.3 g of CuO NPs powder were dispersed separately in 110 mL of distilled water. Each solution was stirred for 60 min at room temperature. The CuO solution was then dispersed using an ultrasonic bath for 1 h at 45 °C. The CuO solution was added dropwise to the silica gel solution and stirred for 60 min. Afterward, the solution was dispersed again with an ultrasonic bath for 15 min at 45 °C. The nanocomposites were separated by centrifugation, washed three times with distilled water, and dried and then dried at 80 °C for 24 h. Finally, the CuO–SiO₂ sample was obtained by calcining the precursor in a furnace at 600 °C for 6 h [45].

Preparation of CuO–SiO₂ sample (Mode-C)

0.3 g of SiO₂ NPs powder and 0.3 g of CuO NPs powder were dissolved separately in 110 mL of distilled water. Each

solution was stirred for 60 min at room temperature. The CuO solution was then dispersed using an ultrasonic bath for 1 h at 45 °C. The CuO solution was added dropwise to the SiO₂ solution and stirred for 60 min. Afterward, the solution was dispersed again with an ultrasonic bath for 15 min at 45 °C. The nanocomposites were separated by centrifugation, washed three times with distilled water, and dried in an oven at 600 °C for 6 h. The resulting dry sediment was ground into a powder.

Characterization of CuO NPs and CuO–SiO₂ NC

Various techniques were employed to comprehensively characterize the CuO–SiO₂ nanocomposites and determine their physical, chemical, and structural properties. UV–Vis spectrophotometry (UV-2450, Shimadzu, Duisburg, Germany) in the range of 200–800 nm confirmed the formation of CuO–SiO₂ nanocomposites. Samples were dispersed in 2 mL of distilled water at a concentration of 0.1 mg. The band gap energy (E_g) was determined using the Tauc relationship $(h\nu) = A(h - E_g)^n$ [46]. Fourier Transform Infrared Spectroscopy (FTIR) (Perkin-Elmer Series 1725X) identified functional groups on the surface within the spectral range of 400–4000 cm⁻¹, elucidating the chemical composition of the nanocomposite.

Additionally, X-ray diffraction (XRD) analysis, conducted with a Rigaku Miniflex 600 device, contributed to understanding the crystal structure and phase composition of the

material, was used to generate the powder X-ray diffraction spectra (XRD) at a scanning rate of 10°/min between 20 and 80°, associated with a Cu radiation source ($\lambda = 1.5405\text{\AA}$) is utilized. Microscopy techniques, specifically scanning electron microscopy (SEM) at 10 kV utilizing a Leo Supra 55 instrument from Zeiss Inc., offered high-resolution images for a detailed examination of the morphology of both CuO nanoparticles and the CuO–SiO₂ nanocomposite. This comprehensive approach allowed for a thorough investigation of the CuO–SiO₂ nanocomposites, combining UV–Vis spectrophotometry, Fourier Transform Infrared Spectroscopy, X-ray diffraction, and scanning electron microscopy to provide a comprehensive understanding of their properties.

Photocatalytic degradation of RB

Photocatalysis utilizing CuO NPs and CuO–SiO₂ nanocomposites has exhibited remarkable efficiency in degrading toxic AZO dyes, such as RB. This eco-friendly process harnesses sunlight to activate the nanoparticles, producing reactive species capable of breaking down the dyes. Consequently, the photocatalytic process not only degrades the dyes but also completely mineralizes them, offering an efficient and sustainable technology for the degradation of dye pollutants [47]. To assess the adsorption capacity, the change in RB dye concentration was measured by comparing the initial aqueous solution with the solution after the photodegradation test [48].

$$qe = \frac{(C_0 - C_e)v}{m} \quad (1)$$

In this context, the equilibrium concentration of the dye adsorbed onto the adsorbent is denoted as qe (mg g⁻¹). The initial and equilibrium concentrations of the dye solution are represented by C_0 and C_t (mg L⁻¹), respectively. Here, m stands for the weight of the CuO NPs used (g), and V represents the volume of the dye solution (L). UV–Vis spectroscopy is employed to monitor the reaction progress. When CuO NPs and CuO–SiO₂ nanocomposites are introduced into the reaction mixture, the dye undergoes catalytic reduction. Equation (2) is utilized to calculate the photodegradation efficiency (%) of the dye RB [46, 49].

$$\text{Degradation ratio(\%)} = \frac{(C_0 - C_t)}{C_0} \times 100 \quad (2)$$

Photocatalytic dye degradation

The catalytic activity of the samples was assessed by observing the photochemical degradation of RB dye in an aqueous solution exposed to sunlight. A dye solution was prepared at a concentration of 2.5×10^{-5} M, with an appropriate amount

of dye catalyst, which was 5.0 mg for both CuO NPs and CuO–SiO₂ nanocomposite. The samples were thoroughly mixed and exposed to direct sunlight. The progression of the reaction was monitored at intervals (5, 15, 30, 45, 60, 75, 90, 105, and 120 min) using a UV–Vis spectrometer. To halt degradation, the solution was centrifuged at 3000 rpm for 5 min, and absorbance was measured at a wavelength of 542 nm for RB using a UV–Vis spectrophotometer.

Results and discussion

UV–Vis spectroscopy

Figure 2a displays the UV–Vis spectra obtained from a *Calligonum comosum* L. extract, unveiling notable peaks detected at wavelengths of 211 nm, 232 nm, and 276 nm. The peak at 211 nm indicates condensed tannins, known for antioxidants [50]. The 232 nm peak suggests flavonoids with various biological benefits [50], and the 276 nm peak implies the presence of polyphenols [50]. Figure 2b presents the UV–Vis spectra of CuO NPs and CuO–SiO₂ nanocomposite using various processes (Mode A, Mode B and Mode C), showing peaks at 280 nm, 285 nm, 209 nm and 207 nm, respectively. The UV–Vis spectra indicate a prominent absorption range between 250 and 300 nm, indicating the successful formation of copper oxide nanoparticles. Notably, a peak at 278 nm is observed, signifying the presence of surface plasmon resonance, which is closely related to the size and shape of the nanoparticles [51]. Using mode A to create the CuO–SiO₂ nanocomposites, the absorption spectra exhibits a peak at 285 nm that is attributable to surface plasmon resonance. This absorption peak, which falls between 280 and 380 nm, is consistent with recent observations from [52–54]. According to Ref [55], the absorbance characteristics of CuO–SiO₂ nanocomposites synthesized in modes B and C display peaks in the region of 200–800 nm, which may be caused by inherent flaws in amorphous SiO₂. In addition, the mesoporous CuO–SiO₂ composite film's UV–Vis absorption spectra exhibits absorption peaks at 210 and 207 nm, respectively, which can be attributed to the O⁻² to Cu⁺² charge-transfer transitions [51, 56]. Additionally, it demonstrates that CuO is present in the mesoporous CuO–SiO₂ composite sheet. The UV–Vis spectra of Fig. 2d showing peak at 296 the absorption spectrum of SiO₂ NPs [57, 58]. Figure 2c shows the band gap energies of CuO NPs and CuO–SiO₂ nanocomposites using different Processes. As an indirect transition semiconductor, CuO is a p -type semiconductor with a band gap 1.42 eV ranging from 1.21 to 1.5 eV [59], for CuO–SiO₂ nanocomposites using different Processes (Mode A, Mode B and Mode C) shows the band gap energies 2.2 eV, 1.80 eV and 3.29 eV respectively, which is larger than that of CuO NPs pur (1.21–1.5 eV). The

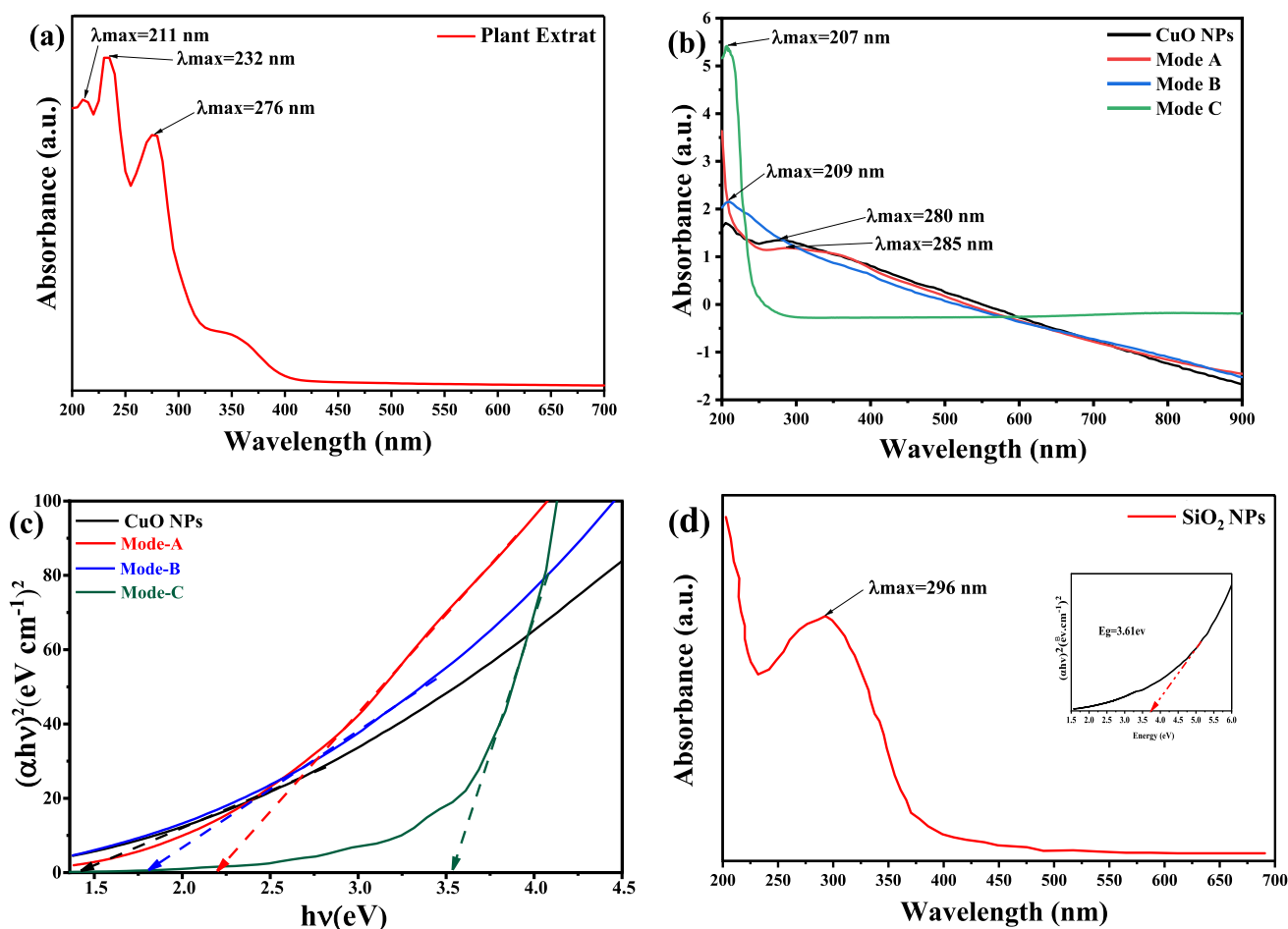


Fig. 2 UV–Vis spectra of the prepared samples: **a** *Calligonum comosum* L. extract *Calligonum comosum* L. extract, **b** CuO NPs and CuO–SiO₂ nanocomposite using different Processes (Mode A, Mode B and Mode C) and **c** curve showing the corresponding optical energy

gap of CuO NPs and CuO–SiO₂ nanocomposite using different Processes (Mode A, Mode B and Mode C), **d** UV–Vis spectra and energy gap of SiO₂ NPs

differing absorption peaks for the CuO NPs and CuO–SiO₂ nanocomposites using different Processes are likely indicative of variations in their electronic structures, bandgap energies, and surface properties. These differences might arise from the incorporation of SiO₂ into the nanocomposite structure show the band gap energies 3.61 eV, leading to alterations in the interaction between light and the materials. This large blue shift for the CuO band gap may result from the quantum size effect of the non-crystalline CuO nanoparticles in the mesoporous composite films [47]

FTIR spectroscopy analysis

FTIR characterization was conducted to identify the functional groups involved in the formation of CuO NPs, SiO₂ NPs, and CuO–SiO₂ nanocomposite using different processes (Mode A, Mode B, and Mode C). In the FT-IR analysis, the spectrum of CuO NPs revealed multiple peaks at

specific wavenumbers: 3445 cm⁻¹, 1655 cm⁻¹, 1575 cm⁻¹, 1088 cm⁻¹, 553 cm⁻¹, and 472 cm⁻¹. As shown in Fig. 3, the CuO nanoparticles exhibit broad absorption bands between 2800 and 4000 cm⁻¹, mainly ascribed to OH- and C–O groups on the surface of the CuO nanostructures [60]. The absorption peaks at 472 cm⁻¹ and 553 cm⁻¹ may be associated with the characteristic stretching vibrations of Cu–O, confirming the CuO phase [61]. The absorption peaks at 3445 and 1655 cm⁻¹ are due to the presence of O–H stretching and bending vibrations [62]. The peak at 1575 cm⁻¹ appeared due to the stretching of aromatic C=C [41]. A broad band at 1088 cm⁻¹ is attributed to CO₂ stretching vibrations from the atmosphere [63]. For pure silica, the IR spectrum displayed strong absorption bands at approximately 1046 cm⁻¹ and 625 cm⁻¹. These bands can be attributed to the asymmetric stretching and rocking vibrations of Si–O–Si bonds in silica, respectively.

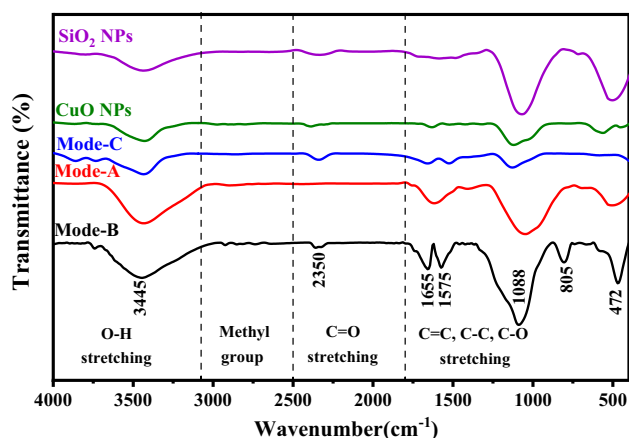


Fig. 3 FTIR spectra of the synthesized the CuO NPs and CuO–SiO₂ nanocomposite using different Processes (Mode A, Mode B and Mode C)

In the IR spectrum of the CuO–SiO₂ nanocomposite, particularly in mode -A, the bands at 491 cm⁻¹ are attributed to Si–O–Si bending and stretching vibrations [64]. Additionally, the bands at 1033 cm⁻¹ were assigned to the Si–O–Si asymmetric stretching vibration [65]. For mode-B: The band at 472 cm⁻¹ is linked to vibrational modes of the silica structure [66]. Furthermore, the bands at 805 cm⁻¹ and 1088 cm⁻¹ are characteristic of Si–O–Si vibrations [67]. In mode-C, the band at 574 cm⁻¹ was assigned to Si–O–Si bending and stretching vibrations [64]. Moreover, there is a band that overlaps with the second one at 1128 cm⁻¹, which is associated with high molecular weight siloxane chains [68].

X-ray diffraction

The XRD spectra shown in Fig. 4 illustrate the distinctive characteristics of both bare CuO NPs and CuO–SiO₂ nanocomposite using different Processes. In Fig. 4a prominent diffraction peaks are observed at specific 2θ values: 32.5°, 35.6°, 38.7°, 46.2°, 48.9°, 53.5°, 58.3°, 61.6°, 66.4°, 68.1°, 72.4° and 75.3°. These peaks correspond to crystal planes (110), (11–1), (111), (11–2), (20–2), (020), (202), (11–3), (310), (220), (311) and (22–2) respectively, which are indicative of the CuO NPs phase (JCPDS no. 00-048-1548). No impurity peaks were observed in the XRD spectra, indicating the high purity of the CuO NPs samples [69]. 19.07° and 32.25° of the SiO₂ structure of amorphous silica were measured at angle 2θ, as well as 28.18° and 29.06°, which indicates that amorphous SiO₂ is usually amorphous. In addition, some small peaks that appeared also showed that sodium (Na) was present in very trace amounts (Fig. 4b).

The incorporation of silicate resulted in the development of additional monoclinic phases of CuO in mode A and

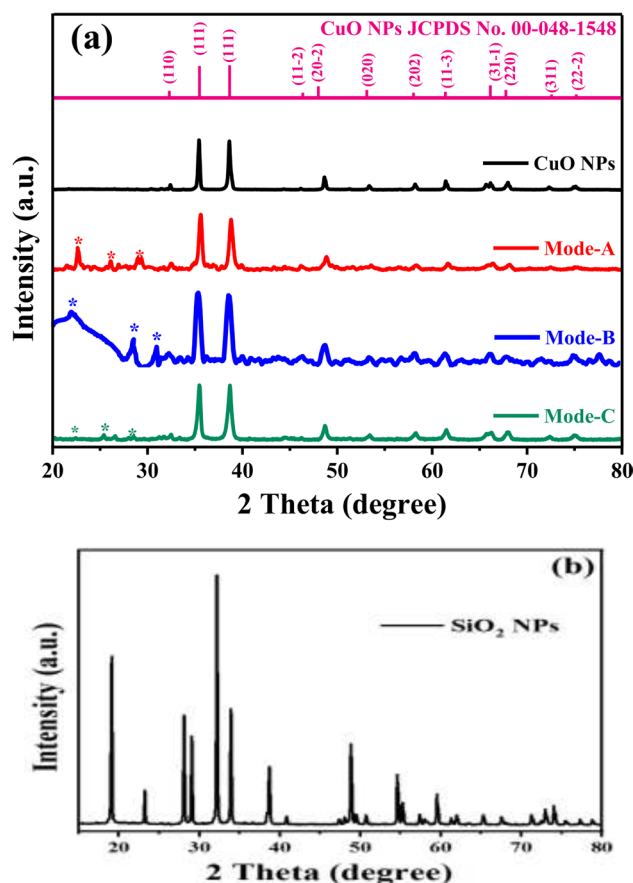


Fig. 4 a XRD pattern of the synthesized CuO NPs and CuO–SiO₂ nanocomposite using different Processes (Mode A, Mode B and Mode C), and b SiO₂ NPs

mode C, indicated by peaks at 2θ values of 22.5°, 25.9°, and 29.1° with the corresponding planes of (101), (110), and (111), respectively. However, in mode B, peaks appeared at 2θ values of 22.1°, 28.7°, and 31.0° with the corresponding planes of (101), (111), and (102), respectively. This Back to a pure SiO₂ NPs with JCPDS no. 01-082-1235 for mode A, mode C and JCPDS no. 01-082-1405 for mode B.

When integrating a layer of CuO NPs with silicate, as illustrated in Fig. 4, it becomes apparent that the crystalline structure of CuO NPs is greatly influenced either by the integration of SiO₂ NPs or during the SiO₂ NPs formation. The average particle size was estimated using the Debye–Scherrer equation [70]:

$$D = \frac{k\lambda}{\beta \cos \theta} \quad (3)$$

where, *d*: the particle size (nm), *k*: is a constant equation to 0.94, *λ*: the wavelength of X-ray radiation (1.5406 Å) and *β* is the full width at half maximum of the diffraction peak (FWHM), *θ* = Bragg's angle.

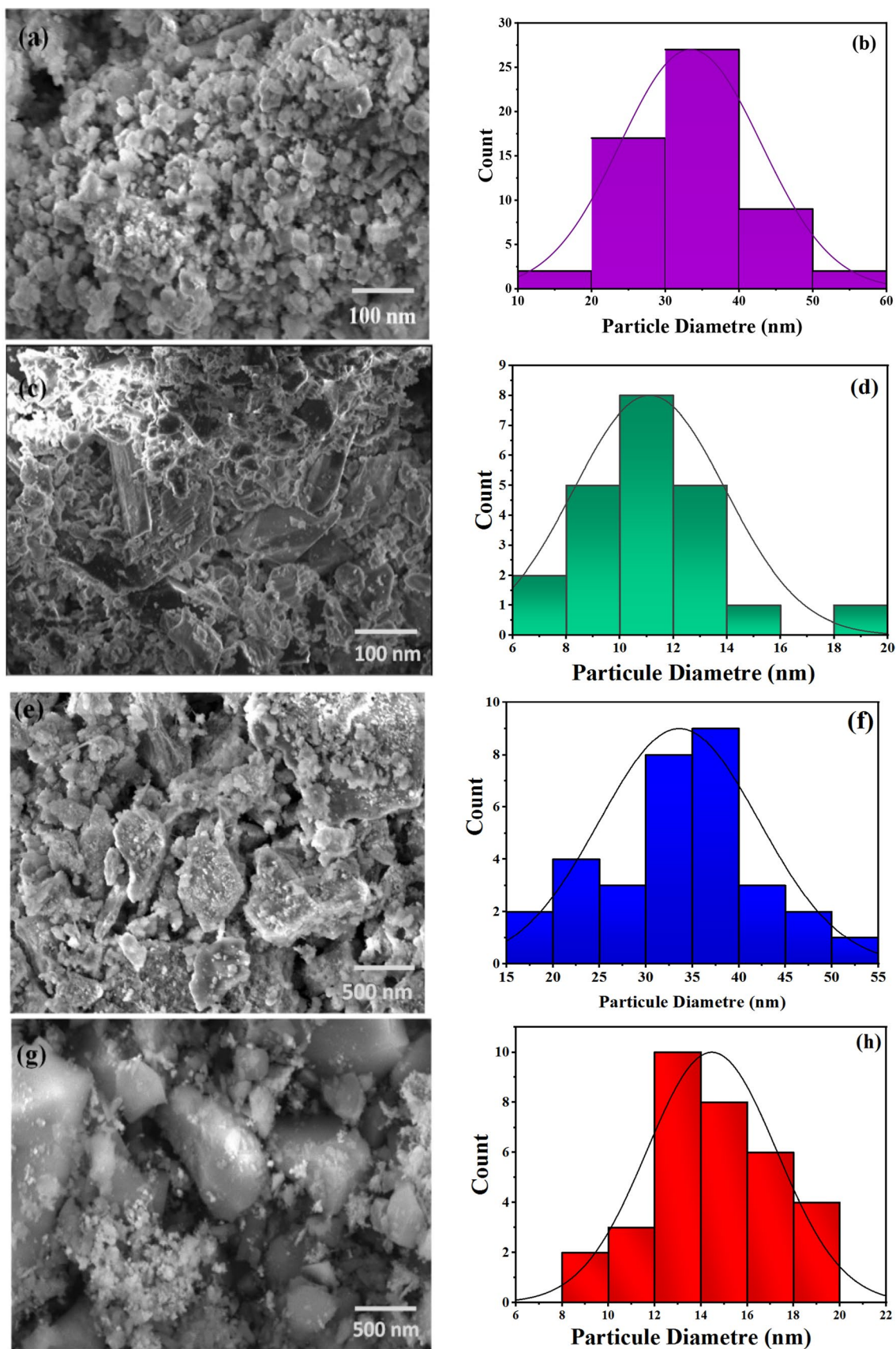


Fig. 5 SEM images and crystallite size distributions: **a, b** CuO NPs, **c, d** SiO₂ NPs, **e, f** CuO-SiO₂ Nanocomposite using Mode-A, **g, h** CuO-SiO₂ Nanocomposite using Mode-B and **k, l** CuO-SiO₂ nanocomposite using Mode-C

The initial measurement of the crystallite size for the standalone pure CuO NPs was found to be 24.4 nm. Subsequently, upon applying a CuO–SiO₂ nanocomposite using different processes (Mode A, Mode B and Mode C), There was a noticeable change in the size of the crystallites. This change led to a decrease in crystallite size, reaching 18.1 nm, 15.6 nm, and 14.8 nm, respectively. This alteration significantly impacted the structural dimensions of the coated CuO NPs. The shift in crystallite size can be attributed to the interactions between CuO and SiO₂ materials. This shift in crystallite size has significant implications for the physical and chemical properties of the coated nanoparticles. It could potentially affect their reactivity, optical features, and overall behavior in diverse applications.

Morphological and elemental analysis

The SEM micrographs and histograms illustrating particle size distribution, as presented in Fig. 5, reveal that the original CuO nanoparticles were made up of consistently spherical particles Fig. 5a [71], ranging in size from 30 to 35 nm. Additionally, the particles silica were observed to have a spherical shape, as depicted in Fig. 5c [72]. The introduction of SiO₂ NPs caused noticeable alterations in the surface morphology of CuO NPs. The SEM images provided clear evidence of increased particle agglomeration, transitioning into structure irregular shapes [65]. This observation confirmed that the presence of SiO₂ particles has the capacity to modify the surface morphology of metal oxides. Compared to Fig. 5e, 5g, k reveals that Mode-B and Mode-C exhibited consists of aggregates of different shapes and sizes, and these particles were smaller and displayed a more uniform size distribution. This outcome can be ascribed to its higher copper content. As the copper loading increased, the atomic arrangement

of CuO_x/SiO₂ may be closer, resulting in smaller particle sizes. As depicted in Fig. 5h, l, this finding aligns with our previous study [73], demonstrating that aggregation and particle growth did not reduce the specific surface area. This suggests that well-structured mesopores were formed.

According to the SEM/EDS elemental analysis presented in Table 1 and Fig. 6, the composition of copper, silicon, and oxygen was determined for the CuO–SiO₂ nanocomposite synthesized by modes (A, B, and C). In mode B, the composition was found to be 22.94% Cu, 18.90% Si, and 58.16% O. In mode C, the composition was 30.10% Cu, 8.65% Si, and 61.25% O. For mode A, the composition included 14.06% Cu, 23.41% Si, and 62.53% O. interestingly, in mode A, silicon and oxygen was where are the major component followed by copper. Conversely, in modes B and C, oxygen and copper were the major's component followed by silicon.

Photocatalytic degradation analysis Rose Bengale

Photocatalytic degradation is a process in which a material, frequently a semiconductor, can absorb light and utilize that energy to initiate chemical reactions. In the context of photocatalytic degradation of dyes, the semiconductor absorbs light, typically in the UV or visible range, thereby generating electron–hole pairs. Figure 7 illustrates the photodegradation process of Rose Bengal (RB) in an aqueous solution using both pure CuO NPs and the CuO–SiO₂ nanocomposite (mode B) under sunlight illumination. These charged particles can engage in redox reactions crucial for the degradation of organic molecules, such as dyes. In Fig. 7a, b, the absorption spectra of pure CuO NPs during the degradation of RB under sunlight exposure are depicted over time. These spectra showcase distinct absorption peaks at approximately 542 nm for RB. As time progresses, these peaks gradually diminish, indicating a slow degradation process that

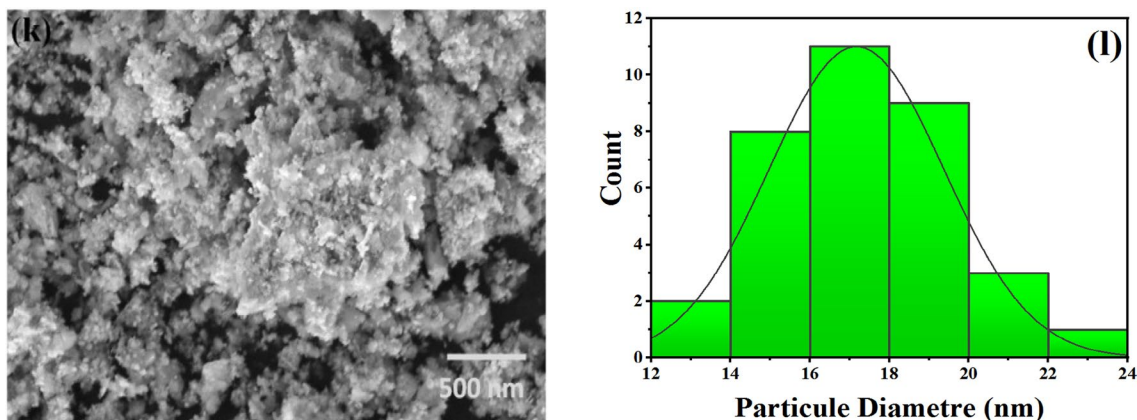


Fig. 5 (continued)

necessitates a considerable amount of time to complete. The photocatalytic activity results demonstrate that CuO NPs achieved a degradation coefficient of 78.8% for RB within a 120 min duration. In contrast, the CuO–SiO₂ nanocomposite exhibited a significantly higher degradation coefficient of 84.8% for RB during the same period. Remarkably, the CuO–SiO₂ nanocomposite had a lower energy gap (1.80 eV), indicating better decomposition efficiency over time. These findings are consistent with several studies [74]

In order to determine the degradation kinetics of Rose bengal (RB) dye, an investigation was carried out on the relationship between $\ln(C_0/C_t)$ and irradiation time, as shown in Fig. 8a, b. It was found that first-order reaction kinetics were respected in the RB degradation reaction, under the catalytic influence of the CuO NPs and CuO–SiO₂ nanocomposite. This means that the rate of the reaction is proportional to the concentration of the remaining dye at any given time. The graphical representation in Fig. 8a, b of $\ln(C_0/C_t)$ versus time provides an overview of the catalytic performance of the CuO NPs and CuO–SiO₂ nanocomposite (NC). The kinetic parameters of RB dye degradation under optimal reaction conditions were examined by plotting the relationship between $\ln(C_0/C_t)$ and time [75, 76]. The linearity between $\ln(C_0/C_t)$ and time in Fig. 8a, b indicates that the reaction follows pseudo-first order kinetics, which can be used to determine how quickly the dye is being degraded. Thus, the reaction rate can be determined by the following equation Eq. (4):

$$\ln\left(\frac{C_0}{C_t}\right) = k_{\text{app}} \times T \quad (4)$$

C_0 denote the initial concentration and C_t is the concentration at time t of the dye or absorption of the RB dye, while k_{app} signifies the rate constant of the reaction (min^{-1}). The apparent rate constant (k_{app}) is determined by computing the slope of the line using the formula mentioned above Eq. (4). These research findings provide additional confirmation of the robust photoreactivity exhibited by the CuO and CuO–SiO₂ catalysts, thereby reaffirming their respective degradation efficiency.

As shown in Table 2, the CuO NPs and CuO–SiO₂ NCs prepared in this study exhibit high AZO dye removal efficiency under visible light irradiation. The removal efficiency for Rose bengal (RB) dye is 78.8% for CuO NPs and 84.8% for CuO–SiO₂ NCs. This is comparable to the removal efficiency reported for other AZO dyes using CuO NPs and CuO–SiO₂ NCs.

Photodegradation mechanism CuO NPs and CuO–SiO₂ NCs

CuO nanoparticles (NPs) and CuO–SiO₂ nanocomposites (NC) exhibit promising potential as photocatalysts for the degradation of organic pollutants when exposed to solar radiation (Fig. 9). The photocatalytic mechanism involves several key steps: firstly, under solar irradiation, electrons within the valence band of CuO NPs and CuO–SiO₂ NC become excited and transition to the conduction band, leaving behind holes in the valence band. Subsequently, these photogenerated electrons and holes migrate to the catalyst's surface [81]. The photogenerated electrons interact with dissolved oxygen, generating superoxide radicals (O_2^-), while the photogenerated holes react with hydroxyl ions (OH^-), forming hydroxyl radicals ($\text{OH}\cdot$). These superoxide and hydroxyl radicals exhibit high reactivity and can effectively oxidize organic pollutants, making them valuable tools for solar-driven photocatalysis [82].

The charge-separation process is essential for the photocatalytic activity of CuO NPs and CuO–SiO₂ NC. If the photogenerated electrons and holes cannot be separated effectively, they will recombine and release the absorbed solar energy as heat, which will reduce the photocatalytic efficiency. The dissolution of H₂O is also important for the photocatalytic process. Water molecules can be oxidized by the photogenerated holes to produce hydroxyl radicals, which are highly reactive and can oxidize organic pollutants. The photocatalytic activity of CuO NPs and CuO–SiO₂ NC can be enhanced by doping with other metals or semiconductors [83, 84]. For example, doping CuO with TiO₂ can improve the charge separation efficiency and increase the surface area of the catalyst, which can lead to enhanced photocatalytic activity [85]. The photocatalytic process of CuO NPs and CuO–SiO₂ NC under solar radiation is a complex process, but it can be summarized in the following steps: excitation of electrons from the valence band to the conduction band, charge separation, generation of superoxide and hydroxyl radicals, and oxidation of organic pollutants by the superoxide and hydroxyl radicals [86, 87].

The mechanism by which the photocatalytic activity is carried out by the catalyst depends on CuO NPs and CuO–SiO₂ NC is based on the generation of hydroxyl radicals ($\bullet\text{OH}$). These radicals are highly reactive and can degrade organic pollutants into smaller, less harmful molecules. A possible mechanism is revealed by the following Eqs. (5–12) [88]:

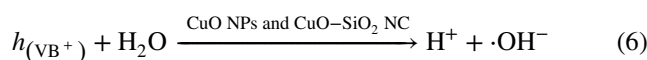
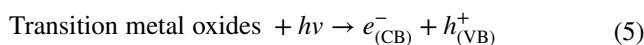
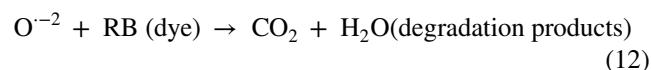
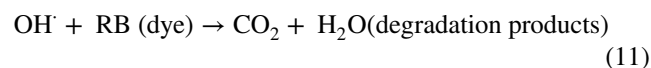
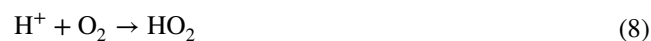
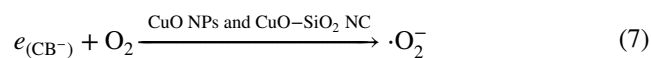


Table 1 lists the weight and atomic percentages of CuO NPs and CuO–SiO₂ nanocomposite using different processes (Mode A, Mode B and Mode C)

Composition of CuO NPs			Composition of CuO–SiO ₂ nanocomposite (Mode A)			Composition of CuO–SiO ₂ nanocomposite (Mode B)			Composition of CuO–SiO ₂ nanocomposite (Mode C)		
Element	Atomic (%)	Weight (%)	Element	Atomic (%)	Weight (%)	Element	Atomic (%)	Weight (%)	Element	Atomic (%)	Weight (%)
O K	66.89	33.72	O K	62.53	39.21	O K	58.16	53.22	O K	61.25	31.25
Cu K	33.11	66.28	Cu K	14.06	35.01	Cu K	22.94	16.42	Cu K	30.10	61.00
			Si K	23.41	25.77	Si K	18.90	30.36	Si K	8.65	7.75



The process begins with the excitation of CuO NPs and CuO–SiO₂ NC by visible light (Eq. 5). This generates electron–hole pairs, which can then migrate to the surface of the photocatalyst. At the surface, the holes can oxidize water to produce hydroxyl radicals (Eq. 6). The electrons can also reduce oxygen to produce superoxide radicals ($\cdot\text{O}_2^-$) (Eq. 7). These superoxide radicals can then react with protons to form hydroperoxyl radicals ($\cdot\text{HO}_2$) (Eq. 8). Two hydroperoxyl radicals can then react to form hydrogen peroxide (H₂O₂) (Eq. 9). Finally, hydrogen peroxide can be photolyzed by visible light to produce two more hydroxyl radicals (Eq. 10).

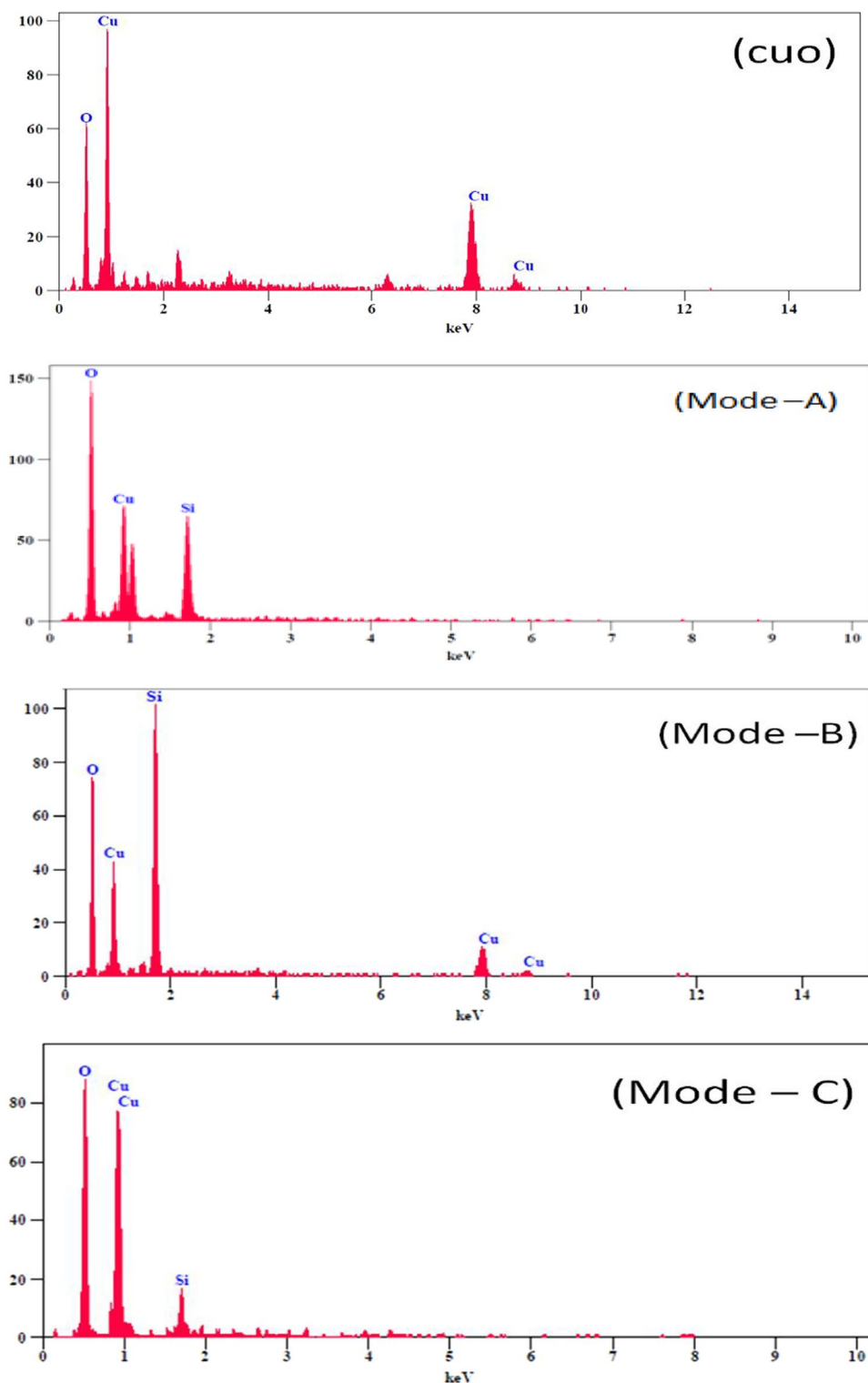
The hydroxyl radicals are the main active species responsible for the photocatalytic degradation of organic pollutants (Eqs. 11, and 12). These radicals can attack and break down organic molecules into smaller, less harmful molecules.

Recyclability and stability

In order to evaluate the recyclability of CuO nanoparticles (NPs) and CuO–SiO₂ nanocomposites (NC) as photocatalysts for water remediation applications. The effectiveness of using CuO NPs and CuO–SiO₂ NC as photocatalysts in water remediation depends on their ability to be separated and reused. To assess their recyclability, the researchers conducted a series of experiments. In each cycle, the used photocatalysts were dried and then employed in a subsequent photocatalysis experiment under the same conditions as the initial cycle.

The results from five consecutive cycles of photocatalyst recycling are shown in Fig. 10a, c. These findings reveal that both CuO NPs and CuO–SiO₂ NC photocatalysts, in their original forms, demonstrated impressive efficiency and reusability in degrading Rose Bengal (RB) dye through photodegradation. Figure 10b, d show that the degradation efficiency of the photocatalysts exhibited a slight decrease, with CuO NPs decreasing from 78.8

Fig. 6 EDX spectrum of CuO NPs and CuO–SiO₂ Nanocomposite using Mode-A, Mode-A, Mode-B and Mode-C, respectively



to 73% and CuO–SiO₂ NC decreasing from 84.8 to 79% after five successful cycles. This decrease is attributed to the inevitable loss of photocatalyst material during the recycling process, likely occurring during washing, centrifugation, or due to the adsorption of certain intermediate species generated during the photocatalysis process

[89, 90]. Figure 10e presents XRD (X-ray diffraction) data, which indicates that the CuO NPs and CuO–SiO₂ NC photocatalysts maintained their essential XRD diffraction peaks both before and after the photodegradation process, throughout the five consecutive photocatalytic cycles. This suggests that the catalytic material did not induce

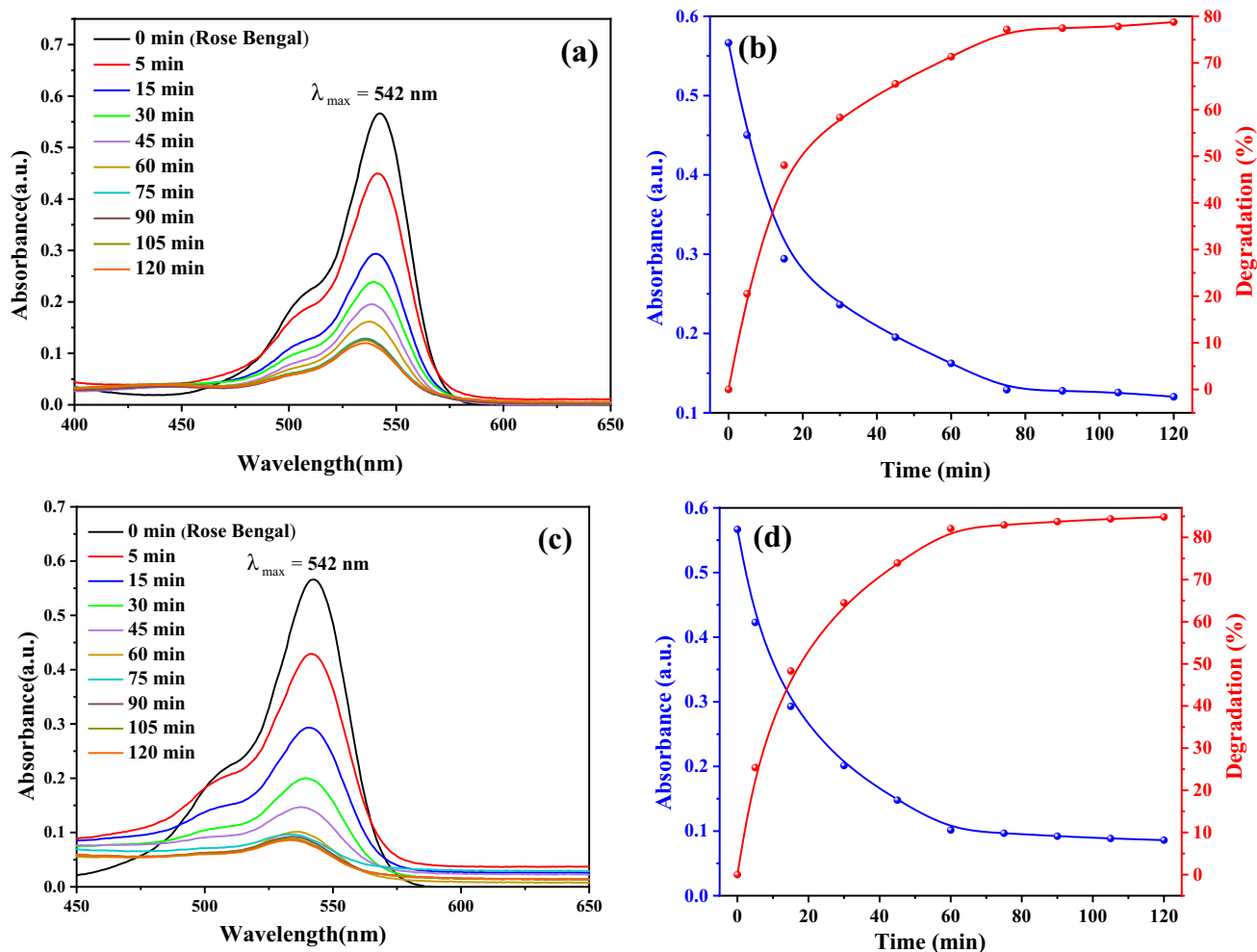


Fig. 7 Photocatalytic behaviour of RB using a, b CuO NPs, c, d CuO–SiO₂ nanocomposite (Mode-B) at different irradiation times under UV/VIS irradiation

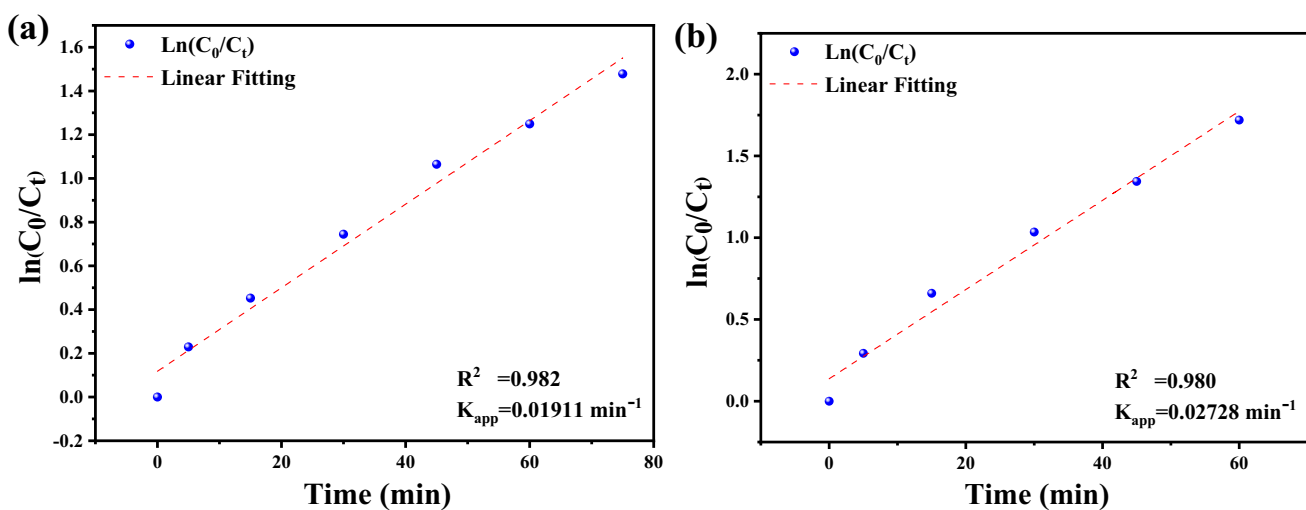
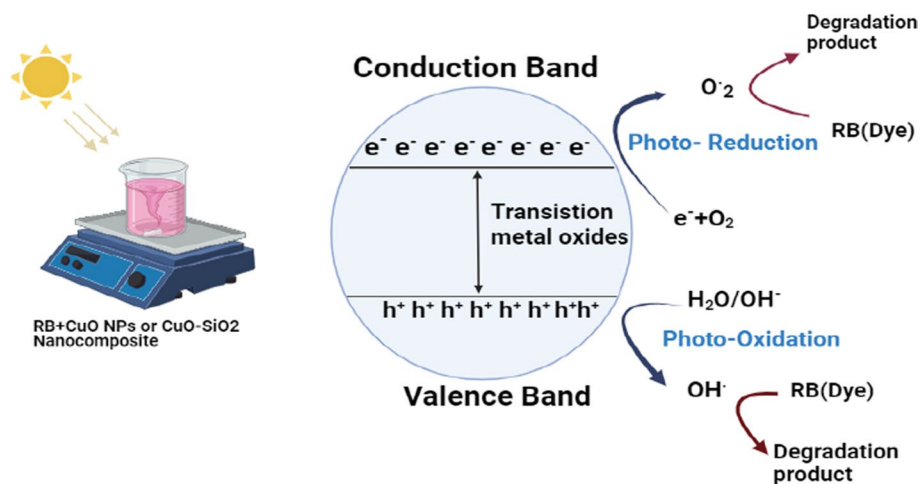


Fig. 8 Plot of $\ln(C_0/C_t)$ versus time for the catalyzed degradation of RB dye by CuO NPs and CuO–SiO₂ nanocomposite: a, b obtained by CuO NPs; c, d obtained by CuO–SiO₂ nanocomposite

Table 2 Comparison of AZO dye removal efficiency results for as-prepared NPs compared to this work

Metal NPs	Method of Synthesis	The particle size (nm)	Band gap (eV)	AZO Dye	Time (min)	Dye removal (%)	Refs.
CuO–SiO ₂	Sol–gel technique	–	2.38–1.91	Acridine orange	30	100	[77]
CuO–SiO ₂	Sol–gel technique	9–10	3.419	Rhodamine B	30	85	[65]
				-Nile Blue		90	
CuO–SiO ₂	Sol–gel	–	3.19	Crystal violet	120	70	[22]
CuO–SiO ₂	Sol–gel	–	3.2–2.8	Rhodamine B	135	92	[78]
CuO NPs	Microwave-assisted green route	23	1.63	Methylene blue	90	98	[79]
CuO NPs	Green method	20–35 nm	1.86 eV	Bromothymol blue (BTB)	3h	100	[41]
CuO NPs	Green method	15.21 nm	1.77 eV	Methylene blue	180	93.4	[80]
CuO NPs	Green method	24.4	1.42	Rose Bengale	120	78.8	This Work
CuO–SiO ₂	Chemical deposition	15.6	1.80			84.8	

Fig. 9 General photodegradation process mechanism

any significant alterations in the diffraction peaks of the CuO NPs and CuO–SiO₂ NC photocatalyst, emphasizing their stability and suitability for reuse in water remediation applications[75].

Conclusion

In this study, CuO–SiO₂ nanocomposites were successfully synthesized using various processes. The crystal sizes of the CuO–SiO₂ nanocomposites (Mode-A, Mode-B, Mode-C) were determined to be 18.1 nm, 15.6 nm, and 14.8 nm, respectively. Additionally, the band gap energies were found to be 2.2 eV, 1.8 eV, and 3.29 eV, respectively. The results suggest that both CuO nanoparticles (NPs) and CuO–SiO₂ nanocomposites (NCs) in their original states displayed impressive efficiency and reusability in photodegrading Rose Bengal (RB) dye. This underscores their stability and suitability for repeated use in water remediation applications. Specifically, in Mode-B, CuO–SiO₂

demonstrated exceptional efficacy in the removal of the organic dye, achieving decomposition coefficients of 84.4% for RB. In comparison, CuO nanoparticles exhibited decomposition coefficients of 78.8%. These results were obtained under specific conditions, including a contact time of 120 min, pH=7, and a solution temperature of 25 °C, all under solar light irradiation. However, the moderate efficiency improvement, from 78 to 84%, suggests that the impact of SiO₂ may be more pronounced over an extended period. The amalgamation of copper oxide (CuO) and silicon dioxide (SiO₂) not only showcases their collaborative benefits but also emphasizes the essential role of innovative materials in contemporary environmental science. Delving into the intricacies of adsorption kinetics, we aim to unravel the complexities and shed light on the exceptional recyclability and stability characteristics displayed by these nanoadsorbents. This research not only strives to extend the current knowledge in nanomaterials and environmental science but also harbors the potential to spark the development of pivotal materials crucial for

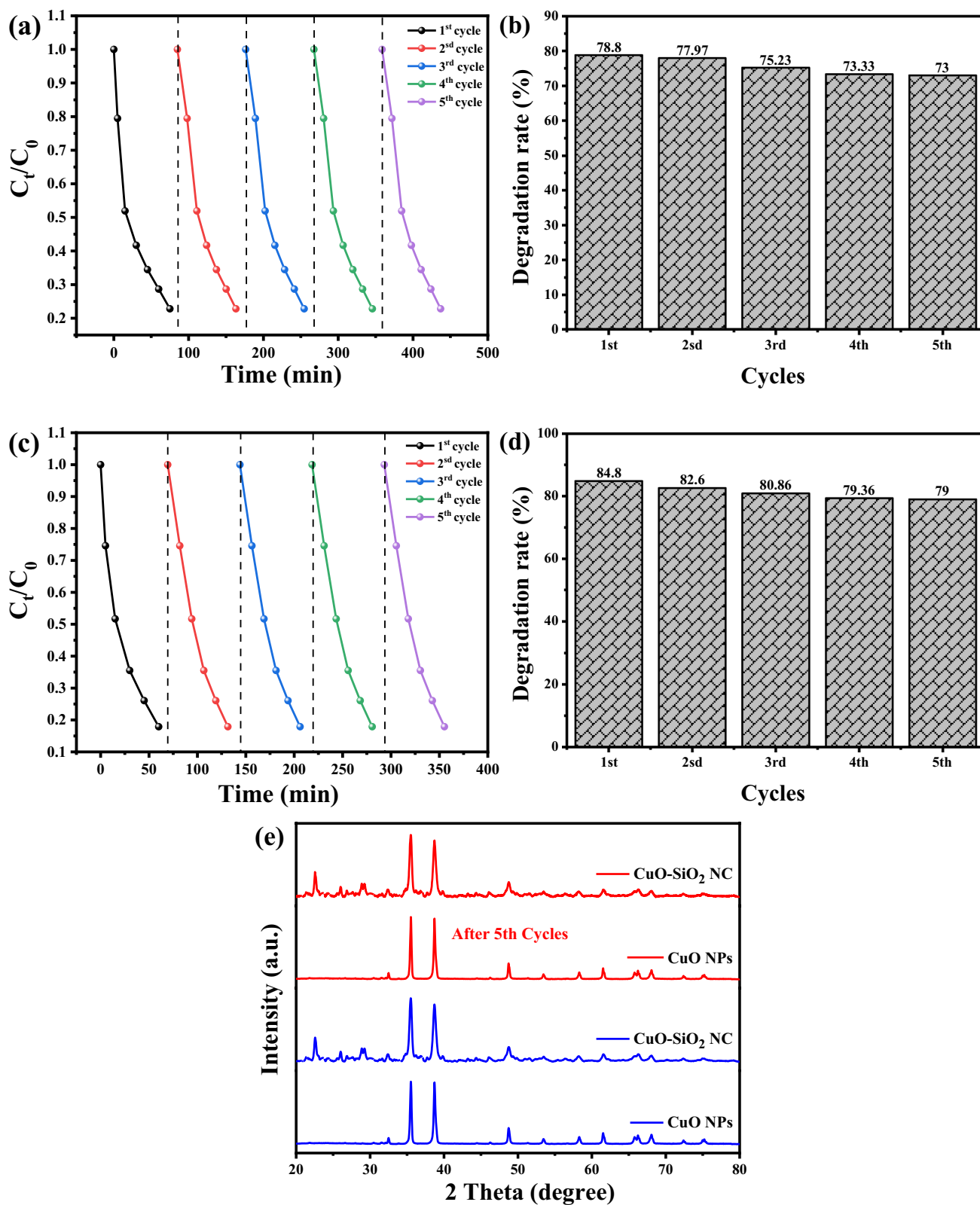


Fig. 10 shows the recyclability of CuO NPs and CuO-SiO₂ NC photocatalysts for degradation of RB dye. **a** CuO NPs, **c** CuO-SiO₂ NC, and **b**, **d** Reusability (degradation) efficiency versus number of cycles

of the photodegradation of RB dye by CuO NPs and CuO-SiO₂ NC, respectively. **e** XRD analysis of CuO NPs and CuO-SiO₂ NC of pure and reused

alleviating the detrimental impact of dye pollutants on ecosystems. Through the lens of this study, our objective is to catalyze further advancements in the field, contributing to ongoing global initiatives for a cleaner, more sustainable future.

Acknowledgements The authors would like to express their sincere gratitude to the Researchers Supporting Project (RSP2024R160), King Saud University (Riyadh, Saudi Arabia) for their support. The authors would also like to thank the Laboratory of Biotechnology Biomaterials and Condensed Matter at the University of El Oued, Algeria for their assistance.

Author contributions Conceptualization: AHG, HH, SEL, AB, IBA, SZ, MTG, FA, ABA; Data curation: SEL, AB, SZ, MTG; Formal analysis: AB, SEL, FA, MTG; Investigation: SEL, AB, SZ, MTG, FA, JAAA, ABA; Methodology: SEL, AB, MTG; Project administration: SEL, MTG; Resources: SEL, MTG, JAAA, AB, SZ; Software: AB, MTG; Supervision: SEL; Validation: AB, SEL, MTG, SZ; Visualization: AB, SEL; Writing—original draft: AB, SEL, JAAA, MTG; Writing—review & editing: AB, SEL, JAAA, MTG; The authors have read and agreed to the published version of the manuscript.

Funding Not Applicable.

Data availability All data generated or analyzed during this study are included in this published article.

Declarations

Conflict of interest The authors declare that they have no competing interests.

Ethical approval Not applicable.

Consent to participate Not applicable.

Consent for publication Not applicable.

Human and animals rights Not applicable.

References

- Chung YT, Ba-Abbad MM, Mohammad AW, Hairom NHH, Benamor A (2015) Synthesis of minimal-size ZnO nanoparticles through sol–gel method: taguchi design optimisation. *Mater Des* 87:780–787
- Amor IB, Hemmami H, Laouini SE, Temam HB, Zaoui H, Barhoum A (2023) Biosynthesis MgO and ZnO nanoparticles using chitosan extracted from *Pimelia Payraudi* Latreille for antibacterial applications. *World J Microbiol Biotechnol* 39(1):1–12
- Khan SA, Noreen F, Kanwal S, Iqbal A, Hussain G (2018) Green synthesis of ZnO and Cu-doped ZnO nanoparticles from leaf extracts of *Abutilon indicum*, *Clerodendrum infortunatum*, *Clerodendrum inerme* and investigation of their biological and photocatalytic activities. *Mater Sci Eng, C* 82:46–59
- Kairyte K, Kadys A, Luksiene Z (2013) Antibacterial and antifungal activity of photoactivated ZnO nanoparticles in suspension. *J Photochem Photobiol, B* 128:78–84
- Naz S, Gul A, Zia M, Javed R (2023) Synthesis, biomedical applications, and toxicity of CuO nanoparticles. *Appl Microbiol Biotechnol* 107(4):1039–1061
- Koffyberg F, Benko F (1982) A photoelectrochemical determination of the position of the conduction and valence band edges of p-type CuO. *J Appl Phys* 53(2):1173–1177
- Weldegebrieal GK (2020) Photocatalytic and antibacterial activity of CuO nanoparticles biosynthesized using *Verbascum thapsus* leaves extract. *Optik* 204:164230
- Balasubramaniam M, Balakumar S (2016) Effect of precipitating agent NaOH on the preparation of copper oxide nanostructures for electrochemical applications. *Наносистемы физика, химия, математика* 7(3):482–487
- Arunkumar V, Jeyakumar SJ, Jothibas M (2019) A sol-gel approach to the synthesis of CuO nanoparticles using *Lantana camara* leaf extract and their photo catalytic activity. *Optik* 183:698–705
- Vinothkumar P, Manoharan C, Shanmugapriya B, Bououdina M (2019) Effect of reaction time on structural, morphological, optical and photocatalytic properties of copper oxide (CuO) nanostructures. *J Mater Sci: Mater Electron* 30:6249–6262
- Aroob S, Carabineiro SA, Taj MB, Bibi I, Raheel A, Javed T, Yahya R, Alelwani W, Verpoort F, Kamwilaisak K (2023) Green synthesis and photocatalytic dye degradation activity of CuO nanoparticles. *Catalysts* 13(3):502
- Kunzmann A, Andersson B, Vogt C, Feliu N, Ye F, Gabrielsson S, Toprak MS, Buerki-Thurnherr T, Laurent S, Vahter M (2011) Efficient internalization of silica-coated iron oxide nanoparticles of different sizes by primary human macrophages and dendritic cells. *Toxicol Appl Pharmacol* 253(2):81–93
- Mohan S, Navamani P, Jayamoorthy K, Srinivasan N (2017) Nano-silica catalyzed synthesis, solvent effect, NMR spectral and DFT studies of some imidazole derivatives. *SILICON* 9:817–822
- Harraz FA, Abdel-Salam OE, Mostafa AA, Mohamed RM, Hanafy M (2013) Rapid synthesis of titania–silica nanoparticles photocatalyst by a modified sol–gel method for cyanide degradation and heavy metals removal. *J Alloy Compd* 551:1–7
- Zhao X, Long R, Chen Y, Chen Z (2010) Synthesis, characterization of CeO₂@ SiO₂ nanoparticles and their oxide CMP behavior. *Microelectron Eng* 87(9):1716–1720
- Khodashenas B, Ghorbani HR (2014) Synthesis of copper nanoparticles: an overview of the various methods. *Korean J Chem Eng* 31:1105–1109
- Khan MS, Khattak R, Khan A, Chen Q, Nisar J, Iqbal Z, Rashid A, Kamran AW, Zekker I, Zahoor M (2021) Synthesis and characterizations of PdNi carbon supported nanomaterials: studies of electrocatalytic activity for oxygen reduction in alkaline medium. *Molecules* 26(11):3440
- Olteanu NL, Lazăr CA, Petcu AR, Meghea A, Rogozea EA, Mihaly M (2016) “One-pot” synthesis of fluorescent Au@ SiO₂ and SiO₂@ Au nanoparticles. *Arab J Chem* 9(6):854–864
- Li X, Yang Z, Hu N, Zhang L, Zhang Y, Yin L (2016) Docetaxel-loaded SiO₂@ Au@ GO core–shell nanoparticles for chemo-photothermal therapy of cancer cells. *RSC Adv* 6(54):48379–48386
- Arreche R, Bellotti N, Blanco M, Vázquez P (2015) Synthesis and characterization of zirconium oxides for use as antimicrobial additives in paints. *Procedia Mater Sc* 9:627–634
- Rebelo QH, Ferreira CS, Santos PL, Bonacin JA, Passos RR, Pocrifka LA, Paula MM (2018) Synthesis and characterization of a nanocomposite NiO/SiO₂ from a sustainable source of SiO₂. *Part Sci Technol* 37(8):911–915
- Yaseen M, Farooq S, Khan A, Shah N, Shah LA, Bibi S, Khan IU, Ahmad S (2022) CuO-SiO₂ based nanocomposites: synthesis, characterization, photocatalytic, antileishmanial, and antioxidant studies. *J Chin Chem Soc* 69(9):1637–1653

23. Kusumawati DH, Putri NP, Hidayat N, Taufiq A, Supardi ZAI (2018) Synthesis and characterization of γ -Al₂O₃/SiO₂ composite materials. *J Phys: Conf Ser* 1:012015
24. Jena KK, Mittal H, Wadi VS, Mani GK, Alhassan SM (2019) Advanced TiO₂–SiO₂–Sulfur (Ti–Si–S) nanohybrid materials: potential adsorbent for the remediation of contaminated wastewater. *ACS Appl Mater Interfaces* 11(33):30247–30258
25. Mobarakeh MI, Saffar-Teluri A, Tabrizi SH (2015) Synthesis and characterization of Al₂O₃–SiO₂–MgO nanocomposite prepared by sol–gel process as an efficient catalyst for the Knoevenagel condensation of aldehydes with malononitrile. *Res Chem Intermed* 41:6625–6633
26. Dippong T, Cadar O, Levei EA, Deac I-G, Borodi G (2018) Formation of CoFe₂O₄/PVA-SiO₂ nanocomposites: effect of diol chain length on the structure and magnetic properties. *Ceram Int* 44(9):10478–10485
27. González-Hurtado M, Marins J, Soares BG, Briones JR, Rodríguez AR, Ortiz-Islas E (2018) Magnetic SiO₂-Fe₃O₄ nanocomposites as carriers of ibuprofen for controlled release applications. *Rev Adv Mater Sci* 55(1):12–20
28. Indriyani A, Yulizar Y, Tri Yunarti R, Oky Bagus Apriandanu D, Marcony Surya R (2021) One-pot green fabrication of BiFeO₃ nanoparticles via *Abelmoschus esculentus* L. leaves extracts for photocatalytic dye degradation. *Appl Surf Sci* 563:150113. <https://doi.org/10.1016/j.apsusc.2021.150113>
29. Marcony Surya R, Mauliddiyah S, Bagus Apriandanu DO, Sudirman YY (2022) SnMnO(3)-decorated ZnO in a hexane-water interface for enhancing visible light-driven photocatalytic degradation of malachite green. *Chemosphere* 304:135125. <https://doi.org/10.1016/j.chemosphere.2022.135125>
30. Sharma A, Kumar N, Sillanpää M, Makgwane PR, Kumar S, Kumari K (2022) Carbon nano-structures and functionalized associates: adsorptive detoxification of organic and inorganic water pollutants. *Inorg Chem Commun* 141:109579. <https://doi.org/10.1016/j.inoche.2022.109579>
31. Sharma A, Makgwane PR, Lichtfouse E, Kumar N, Bandegharai AH, Tahir M (2023) Recent advances in synthesis, structural properties, and regulation of nickel sulfide-based heterostructures for environmental water remediation: an insight review. *Environ Sci Pollut Res Int* 30(24):64932–64948. <https://doi.org/10.1007/s11356-023-27093-z>
32. Apriandanu DOB, Yulizar Y (2021) CuO-bentonite-gold nanocomposites: facile green preparation and their characterization. *Mater Lett* 284:128911. <https://doi.org/10.1016/j.matlet.2020.128911>
33. Apriandanu DOB, Yulizar Y (2019) *Tinospora crispa* leaves extract for the simple preparation method of CuO nanoparticles and its characterization. *Nano-Struct Nano-Objects* 20:100401. <https://doi.org/10.1016/j.nanos.2019.100401>
34. Kumari V, Sharma A, Kumar N, Sillanpää M, Makgwane PR, Ahmaruzzaman M, Hosseini-Bandegharai A, Rani M, Chinamuthu P (2023) TiO₂-CeO₂ assisted heterostructures for photocatalytic mitigation of environmental pollutants: a comprehensive study on band gap engineering and mechanistic aspects. *Inorg Chem Commun* 151:110564. <https://doi.org/10.1016/j.inoche.2023.110564>
35. Adane T, Adugna AT, Alemayehu E (2021) Textile industry effluent treatment techniques. *J Chem* 2021:5314404. <https://doi.org/10.1155/2021/5314404>
36. Yulizar Y, Abdullah I, Surya RM, Alifa NL (2023) Green synthesis of novel YMnO(3)-doped TiO(2) for enhanced visible-light-driven photocatalytic degradation of malachite green. *J Environ Manage* 342:118139. <https://doi.org/10.1016/j.jenvman.2023.118139>
37. Elviera YY, Apriandanu DOB, Marcony Surya R (2022) Fabrication of novel SnWO₄/ZnO using *Muntingia calabura* L leaf extract with enhanced photocatalytic methylene blue degradation under visible light irradiation. *Ceram Int* 48(3):3564–3577. <https://doi.org/10.1016/j.ceramint.2021.10.135>
38. Tripathi M, Singh S, Pathak S, Kasaudhan J, Mishra A, Bala S, Garg D, Singh R, Singh P, Singh PK, Shukla AK, Pathak N (2023) Recent Strategies for the remediation of textile dyes from wastewater: a systematic review. *Toxics*. <https://doi.org/10.3390/toxics11110940>
39. Kaur A, Sharma S (2018) Various methods for removal of dyes from industrial effluents—a review. *Indian J Sci Technol* 11(12):1–21. <https://doi.org/10.17485/ijst/2018/v11i12/120847>
40. Kathing C, Saini G (2022) A review of various treatment methods for the removal of dyes from textile effluent. *Recent Progr Mater* 04(04):028. <https://doi.org/10.21926/rpm.2204028>
41. Prakash S, Elavarasan N, Venkatesan A, Subashini K, Sowndharya M, Sujatha V (2018) Green synthesis of copper oxide nanoparticles and its effective applications in Biginelli reaction, BTB photodegradation and antibacterial activity. *Adv Powder Technol* 29(12):3315–3326
42. Sharma JK, Akhtar MS, Ameen S, Srivastava P, Singh G (2015) Green synthesis of CuO nanoparticles with leaf extract of *Calotropis gigantea* and its dye-sensitized solar cells applications. *J Alloy Compd* 632:321–325
43. Kouadri I, Seghir BB, Hemmami H, Zeghoud S, Allag N, Rebiai A, Amor IB, Chala A, Belkhalifa H (2023) Extraction of silica from different sources of agricultural waste. *Asian J Res Chem* 16(1):98–102
44. Niu X, Zhao T, Yuan F, Zhu Y (2015) Preparation of hollow CuO@ SiO₂ spheres and its catalytic performances for the NO+CO and CO oxidation. *Sci Rep* 5(1):9153
45. Alfaro A, León A, Guajardo-Correa E, Reuquen P, Torres F, Mery M, Segura R, Zapata PA, Orihuela PA (2019) MgO nanoparticles coated with polyethylene glycol as carrier for 2-Methoxyestradiol anticancer drug. *PLoS ONE* 14(8):e0214900
46. Ben Amor I, Hemmami H, Laouini SE, Mahboub MS, Barhoum A (2022) Sol–gel synthesis of ZnO nanoparticles using different chitosan sources: effects on antibacterial activity and photocatalytic degradation of AZO dye. *Catalysts* 12(12):1611
47. Rao VN, Kwon H, Lee Y, Ravi P, Ahn CW, Kim K, Yang J-M (2023) Synergistic integration of MXene nanosheets with CdS@TiO₂ core@ shell S-scheme photocatalyst for augmented hydrogen generation. *Chem Eng J* 471:144490
48. Li Q, Xue D-X, Zhang Y-F, Zhang Z-H, Gao Z, Bai J (2017) A dual-functional indium–organic framework toward organic pollutant decontamination via physically selective adsorption and chemical photodegradation. *J Mater Chem A* 5(27):14182–14189
49. Pang YL, Law ZX, Lim S, Chan YY, Shuit SH, Chong WC, Lai CW (2021) Enhanced photocatalytic degradation of methyl orange by coconut shell–derived biochar composites under visible LED light irradiation. *Environ Sci Pollut Res* 28:27457–27473
50. Amarowicz R, Weidner S, Wójtowicz I, Karmac M, Kosinska A, Rybarczyk A (2010) Influence of low-temperature stress on changes in the composition of grapevine leaf phenolic compounds and their antioxidant properties. *Funct Plant Sci Biot* 4:90–96
51. Wang YM, Wu ZY, Shi LY, Zhu JH (2005) Rapid functionalization of mesoporous materials: directly dispersing metal oxides into as-prepared SBA-15 occluded with template. *Adv Mater* 17(3):323–327
52. Tenkyong T, Bachan N, Raja J, Kumar PN, Shyla JM (2015) Investigation of sol-gel processed CuO/SiO₂ nanocomposite as a potential photoanode material. *Mater Sci-Pol* 33(4):826–834
53. Abba E, Shehu Z, Haruna RM (2021) Green synthesis and characterization of CuO@ SiO₂ nanocomposite using gum Arabic (*Acacia senegalensis*)(L) against malaria vectors. *Trends Sci* 18(19):28–28

54. Cahyana A, Sari S, Ardiansah B (2019) Catalytic performance of CuO@ SiO₂ for one-pot synthesis of pyrimidine derivative, ethyl 6-methyl-2-oxo-4-phenyl-1, 2, 3, 4-tetrahydropyrimidine-5-carboxylate. *IOP Conf Ser Mater Sci Eng* 1:012052
55. Pacchioni G, Ieraño G (1998) Ab initio theory of optical transitions of point defects in SiO₂. *Phys Rev B* 57(2):818
56. Prasetyanto EA, Lee S, Park S (2007) Highly dispersed CuO nanoparticles on SBA-16 type mesoporous silica with cyclam SBA-16 as a precursor. *Bull-Korean Chem Soc* 28(12):2359
57. Biradar AI, Sarvalkar PD, Teli SB, Pawar C, Patil P, Prasad NR (2021) Photocatalytic degradation of dyes using one-step synthesized silica nanoparticles. *Mater Today: Proc* 43:2832–2838
58. Bouibed A, Doufnoune R, Ponçot M (2020) An easy and innovative one-step in situ synthesis strategy of silica nanoparticles decorated by graphene oxide particles through covalent linkages. *Mater Res Express* 6(12):12501254
59. Marabelli F, Parravicini G, Salghetti-Drioli F (1995) Optical gap of CuO. *Phys Rev B* 52(3):1433
60. Padil VVT, Černík M (2013) Green synthesis of copper oxide nanoparticles using gum karaya as a biotemplate and their antibacterial application. *Int J Nanomed* 8:889–898
61. Rahman A, Ismail A, Jumbianti D, Magdalena S, Sudrajat H (2009) Synthesis of copper oxide nano particles by using *Phormidium cyanobacterium*. *Indones J Chem* 9(3):355–360
62. Azam A, Ahmed AS, Oves M, Khan MS, Habib SS, Memic A (2012) Antimicrobial activity of metal oxide nanoparticles against Gram-positive and Gram-negative bacteria: a comparative study. *Int J Nanomed* 7:6003–6009
63. Jayakumar G, Irudayaraj AA, Raj AD (2017) Photocatalytic degradation of methylene blue by nickel oxide nanoparticles. *Mater Today: Proc* 4(11):11690–11695
64. Cruz RSD, Silva JMds, Arnold U, Sercheli MS, Schuchardt U (2002) Copper containing silicates as catalysts for liquid phase cyclohexane oxidation. *J Braz Chem Soc* 13:170–176
65. Yaseen M, Humayun M, Khan A, Idrees M, Shah N, Bibi S (2022) Photo-assisted removal of rhodamine b and Nile blue dyes from water using CuO–SiO₂ composite. *Molecules* 27(16):5343
66. Putz A-M, Putz MV (2012) Spectral inverse quantum (Spectral-IQ) method for modeling mesoporous systems: application on silica films by FTIR. *Int J Mol Sci* 13(12):15925–15941
67. Tellez L, Rubio J, Rubio F, Morales E, Oteo J (2003) Synthesis of inorganic-organic hybrid materials from TEOS, TBT and PDMS. *J Mater Sci* 38:1773–1780
68. Demjen Z, Pukanszky B, Földes E, Nagy J (1997) Interaction of silane coupling agents with CaCO₃. *J Colloid Interface Sci* 190(2):427–436
69. Abebe B, Tsegaye D, Sori C, Renuka Prasad RC, Murthy HA (2023) Cu/CuO-doped ZnO nanocomposites via solution combustion synthesis for catalytic 4-nitrophenol reduction. *ACS Omega* 8(10):9597–9606
70. Berra D, Laouini S, Benhaoua B, Ouahrani M, Berrani D, Rahal A (2018) Green synthesis of copper oxide nanoparticles by *Phoenix dactylifera* L leaves extract. *Dig J Nanomater Biostruct* 13(4):1231–1238
71. Chowdhury R, Khan A, Rashid MH (2020) Green synthesis of CuO nanoparticles using *Lantana camara* flower extract and their potential catalytic activity toward the aza-Michael reaction. *RSC Adv* 10(24):14374–14385
72. Justine M, Prabu HJ, Johnson I, Raj DMA, Sundaram SJ, Kaviyarasu K (2021) Synthesis and characterizations studies of ZnO and ZnO–SiO₂ nanocomposite for biodiesel applications. *Mater Today: Proc* 36:440–446
73. Chen M, Tsai Y, Tseng C, Lin H, Hsi H (2019) Using rice-husk-derived porous silica modified with recycled Cu from industrial wastewater and Ce to remove Hg⁰ and NO from simulated flue gases. *Aerosol Air Qual Res* 19:2557–2567
74. Li Z, Liu G, Su Q, Lv C, Jin X, Wen X (2019) UV-induced photodegradation of naproxen using a nano γ -FeOOH composite: degradation kinetics and photocatalytic mechanism. *Front Chem* 7:847
75. Meneceur S, Bouafia A, Laouini SE, Mohammed HA, Daoudi H, Chami S, Hasan GG, Abdullah JAA, Salmi C (2023) Removal efficiency of heavy metals, oily in water, total suspended solids, and chemical oxygen demand from industrial petroleum wastewater by modern green nanocomposite methods. *J Environ Chem Eng*. <https://doi.org/10.1016/j.jece.2023.111209>
76. Meneceur S, Bouafia A, Laouini SE, Mohammed HA, Daoudi H, Hasan GG, Salmi C (2023) High-efficiency photocatalytic degradation of antibiotics and molecular docking study to treat the omicron variant of COVID-19 infection using biosynthesized ZnO@Fe₃O₄ nanocomposites. *Phys Scr* 98:115926. <https://doi.org/10.1088/1402-4896/acff2d>
77. Gadah R, Basaleh A (2020) Influence of doped platinum nanoparticles on photocatalytic performance of CuO–SiO₂ for degradation of Acridine orange dye. *Ceram Int* 46(2):1690–1696
78. Lims SC, Divya S, Jose M (2023) Design of CuO@ SiO₂ core shell nanocomposites and its applications to photocatalytic degradation of Rhodamine B dye. *Opt Mater* 144:114356
79. Kannan K, Radhika D, Vijayalakshmi S, Sadasivuni KK, Ojiaku A, Verma U (2022) Facile fabrication of CuO nanoparticles via microwave-assisted method: photocatalytic, antimicrobial and anticancer enhancing performance. *Int J Environ Anal Chem* 102(5):1095–1108
80. Atri A, Echabaane M, Bouzidi A, Harabi I, Soucase BM, Chaâbane RB (2023) Green synthesis of copper oxide nanoparticles using *Ephedra Alata* plant extract and a study of their antifungal, antibacterial activity and photocatalytic performance under sunlight. *Heliyon* 9(2):e13484
81. Kir I, Laouini SE, Meneceur S, Bouafia A, Mohammed HAM (2023) Biosynthesis and characterization of novel nanocomposite ZnO/BaMg₂ efficiency for high-speed adsorption of AZO dye. *Biomass Convers Biorefin*. <https://doi.org/10.1007/s13399-023-03985-5>
82. Bouafia A, Meneceur S, Chami S, Laouini SE, Daoudi H, Legmairi S, Mohammed Mohammed HA, Aoun N, Menaa F (2023) Removal of hydrocarbons and heavy metals from petroleum water by modern green nanotechnology methods. *Sci Rep* 13:5637. <https://doi.org/10.1038/s41598-023-32938-1>
83. Gherbi B, Laouini SE, Meneceur S, Bouafia A, Hemmami H, Tedjani ML, Thiripuranathar G, Barhoum A, Menaa F (2022) Effect of pH value on the bandgap energy and particles size for biosynthesis of ZnO nanoparticles: efficiency for photocatalytic adsorption of methyl orange. *Sustainability (Switzerland)* 14:11300. <https://doi.org/10.3390/su141811300>
84. Legmairi S, Meneceur S, Bouafia A, Laouini SE, Alshareef SA, Al-Essa K, Almukhlifi HA, Tedjani ML, Menaa F (2023) Biofabrication of NiO and NiO-decorated Fe nanocomposite efficiency for removal of methylene blue from aqueous solution. *Biomass Convers Biorefin*. <https://doi.org/10.1007/s13399-023-03912-8>
85. Ahmadiasl R, Moussavi G, Shekoohian S, Razavian F (2022) Synthesis of Cu-doped TiO₂ nanocatalyst for the enhanced photocatalytic degradation and mineralization of gabapentin under UVA/LED irradiation: characterization and photocatalytic activity. *Catalysts* 12(11):1310. <https://doi.org/10.3390/catal12111310>
86. Laouini SE, Bouafia A, Soldatov AV, Algarni H, Tedjani ML, Ali GAM, Barhoum A (2021) Green synthesized of ag/ag₂O nanoparticles using aqueous leaves extracts of *Phoenix dactylifera* L and their azo dye photodegradation. *Membranes* 11:468. <https://doi.org/10.3390/membranes11070468>
87. Meneceur S, Hemmami H, Bouafia A, Laouini SE, Tedjani ML, Berra D, Mahboub MS (2022) Photocatalytic activity of iron

- oxide nanoparticles synthesized by different plant extracts for the degradation of diazo dyes Evans blue and Congo red. *Biomass Convers Biorefin.* <https://doi.org/10.1007/s13399-022-02734-4>
88. Kannadasan N, Shanmugam N, Cholan S, Sathishkumar K, Viruthagiri G, Poonguzhali RJMC (2014) The effect of Ce⁴⁺ incorporation on structural, morphological and photocatalytic characters of ZnO nanoparticles. *Mater Charact* 97:37–46
89. El-Berry MF, Sadeek SA, Abdalla AM, Nassar MY (2021) Microwave-assisted fabrication of copper nanoparticles utilizing different counter ions: an efficient photocatalyst for photocatalytic degradation of safranin dye from aqueous media. *Mater Res Bull* 133:111048. <https://doi.org/10.1016/j.materresbull.2020.111048>
90. Ali Baig AB, Rathinam V, Ramya V (2021) Facile fabrication of Zn-doped SnO₂ nanoparticles for enhanced photocatalytic

dye degradation performance under visible light exposure. *Adv Compos Hybrid Mater* 4:114–126. <https://doi.org/10.1007/s42114-020-00195-9>

Publisher's Note Springer Nature remains neutral with regard to jurisdictional claims in published maps and institutional affiliations.

Springer Nature or its licensor (e.g. a society or other partner) holds exclusive rights to this article under a publishing agreement with the author(s) or other rightsholder(s); author self-archiving of the accepted manuscript version of this article is solely governed by the terms of such publishing agreement and applicable law.